Rare Metal Materials and Engineering
Volume 53, Issue 7, July 2024
Available online at www.rmme.ac.cn

Science Press

Cite this article as: Zhao Yanchun, Song Haizhuan, Ma Huwen, et al. Effect of Cu Content on Corrosion Resistance and Antibacterial Properties of Iron-Based Medium Entropy Alloy[J]. Rare Metal Materials and Engineering, 2024, 53(07): 1817-1825. DOI: 10.12442/j.issn.1002-185X.20230636.

ARTICLE

Effect of Cu Content on Corrosion Resistance and Antibacterial Properties of Iron-Based Medium Entropy Alloy

Zhao Yanchun[1,2], Song Haizhuan[1], Ma Huwen[1], Hu Ruonan[1], Feng Li[1,2], Duan Wangchun[3], Liaw Peter K[4]

[1] State Key Laboratory of Advanced Processing and Recycling of Non-ferrous Metals, Lanzhou University of Technology, Lanzhou 730050, China; [2] Wenzhou Pump and Valve Engineering Research Institute, Lanzhou University of Technology, Wenzhou 325105, China; [3] Lanzhou Resources & Environment Voc-tech University, Lanzhou 730123, China; [4] Department of Materials Science and Engineering, University of Tennessee, Knoxville TN 37996, USA

Abstract: $(Fe_{63.3}Mn_{14}Si_{9.1}Cr_{9.8}C_{3.8})_{99.5-x}Cu_xAg_{0.5}$ (x=1, 2, 3, 4, 5, at%) alloys were prepared by water-cooled copper crucible magnetic levitation vacuum melting furnace. The effects of Cu contents on microstructure, corrosion resistance, and antibacterial performance of the alloys were investigated. The results show that the medium entropy alloys possess fcc phase after solid solution and aging treatment. With the increase in Cu content, the Cu-enriched and Ag-enriched fcc2 phase is precipitated on the fcc1 Fe-rich matrix. The corrosion resistance of the alloys in 3.5wt% NaCl solution is superior to that of AISI304. The corrosion current density first decreases and then increases, and the impedance arc radius first increases and then decreases, indicating an initial enhancement and subsequent weakening of the corrosion resistance as the Cu content increases. Moreover, the corrosion rate of the alloys in Escherichia coli suspension shows a trend of increasing first and then decreasing. When x=2 the alloy exhibits the best corrosion resistance, and there is a trade-off effect between the corrosion resistance and antibacterial performance. The fcc2 phase effectively enhances the antibacterial performance of the alloy, and the alloy of x=5 shows the optimal antibacterial rate of 99.94%.

Key words: medium entropy alloys; microstructure; corrosion behavior; antibacterial property

Medium and high entropy alloys possess a unique "cocktail" effect, so adding elements with anticorrosive properties can improve the corrosion resistance of the alloy without sacrificing mechanical properties[1]. Alloying can intervene the formation of passivation film and thus control the corrosion resistance property of the alloy via different phases and element segregation[2–3]. Several studies on the corrosion performance of Cu-containing high entropy alloys have been reported, such as CoCrCuFeNi, CrCuFeMnNi, and CoCrCuFeMn alloys[4–6]. Hsu et al[7] found that adding Cu to CoCrFeNi alloy results in the formation of Cu-rich interdendritic phases, causing galvanic corrosion and reducing the corrosion resistance of the alloy. Kato et al[8] prepared Cu-containing high entropy alloy CoCrCuFeNi with Cu content ranging from 0% to 5% and mainly studied the corrosion behavior of the alloy in 1 mol/L NaCl solution. The results show that Cu mainly exists in the form of CuO in the oxide film, and the pitting potential of $CoCrCu_1FeNi$ alloy is higher than that of CoCrCuFeNi alloy, showing the best corrosion performance. Moreover, there is a growing interest in developing metal materials that are both corrosion-resistant and antimicrobial for epidemic prevention. Researchers have aging treated antimicrobial stainless steel containing Cu to ensure that more Cu-rich phases can precipitate from the alloy, as the Cu-rich phases in the alloy act as cathodes and form galvanic couples with the alloy matrix, resulting in the release of sufficient Cu ions during the reaction process, thereby imparting good antimicrobial properties to the alloy[6]. However, the generation of excessive Cu-rich phases in the alloy will have a detrimental effect on the passivation film of

Received date: October 11, 2023
Foundation item: Zhejiang Provincial Natural Science Foundation (LY23E010002); National Natural Science Foundation of China (52061027); Science and Technology Program Project of Gansu Province (22YF7GA155, 22CX8GA109); Lanzhou Youth Science and Technology Talent Innovation Project (2023-QN-91); Higher Education Research Project of Lanzhou University of Technology (GJ2021A-4)
Corresponding author: Zhao Yanchun, Ph. D., Professor, State Key Laboratory of Advanced Processing and Recycling of Non-ferrous Metals, Lanzhou University of Technology, Lanzhou 730050, P. R. China, E-mail: zhaoyanchun@edu.lut.cn

the alloy, and the more the Cu-rich phases, the lower the pitting corrosion resistance and intergranular corrosion resistance of the alloy. Therefore, for ensuring both good antimicrobial performance and corrosion resistance of the alloy, appropriate control of the Cu content in the alloy is required.

The main elements of medium entropy alloys are typically only 2 – 4 kinds, with configurational entropy ranging from 1*R* to 1.5*R*. Medium entropy alloys possess comparable mechanical properties to high entropy alloys, and exhibit even better corrosion resistance. Due to these advantages and the ease of industrial application, medium entropy alloys have potential for various applications in the fields such as aerospace, medical, and new energy[9]. Based on this, Cu and Ag elements were added to the Fe-base medium entropy alloy in this study. The alloy was subjected to solution treatment followed by aging treatment. The effect of Cu content on the corrosion resistance and antibacterial properties of the alloy was investigated based on the microstructure characterization, and a medium entropy alloy with excellent corrosion resistance and antibacterial properties was developed.

1 Experiment

The raw materials used in the experiment were metal particles of Fe, Mn, Si, Cr, C, Cu, and Ag with a purity higher than 99.9%. The nominal composition of the medium entropy alloy samples was $(Fe_{63.3}Mn_{14}Si_{9.1}Cr_{9.8}C_{3.8})_{99.5-x}Cu_xAg_{0.5}$ (x=1, 2, 3, 4, 5, at%). The alloy samples were prepared in a water-cooled copper crucible vacuum levitation melting furnace. After solution treatment at 1000 °C for 30 min, the samples were water-quenched and then kept in a heat treatment furnace at 600 °C for 6 h, followed by cooling to room temperature.

The microstructure of alloy samples was analyzed by EMPYREAN X-ray diffractometer (XRD), QUANTA FEG 450 scanning electron microscope (SEM), and energy-dispersive X-ray spectroscope (EDS). Corrosion behavior testing was conducted in 3.5wt% NaCl solution, and the anodic polarization curve was measured by a CH166E electrochemical workstation with platinum electrode as the auxiliary electrode and Ag|AgCl|Cl^- as the reference electrode. After the experiment, the corrosion morphology of the alloy was observed by SEM, and the corrosion products were analyzed by Thermo Scientific K-Alpha+ X-ray photoelectron spectrometer (XPS). The antibacterial properties of the alloy samples were tested by the film covering method, and the antibacterial rate was calculated through plate counting method. During the testing period, three parallel samples were prepared, and the antibacterial rate (R) of the alloy was calculated by counting the number of viable bacteria on the plate[10]:

$$R = (B - A)/B \times 100\% \quad (1)$$

where A is the number of viable bacteria in the antimicrobial sample (CFU/mL), and B is the number of viable bacteria in the blank sample (CFU/mL).

2 Results and Discussion

2.1 Microstructure of medium entropy alloy

XRD patterns of Fe-based medium entropy alloy after heat treatment are shown in Fig. 1. The alloy $(Fe_{63.3}Mn_{14}Si_{9.1}Cr_{9.8}C_{3.8})_{99.5-x}Cu_xAg_{0.5}$ mainly exhibits fcc structure. When the Cu content is 1at% and 2at%, Cu can dissolve in the matrix alloy, forming a single-phase solid solution with fcc structure. With further increasing the Cu content, two fcc structures appear when x=3, x=4, and x=5, which are composed of fcc1 phase and fcc2 phase. The intensity of fcc1 diffraction peaks on the (111) plane decreases, while the intensity of fcc2 diffraction peaks increases, indicating that the increase in Cu content promotes the formation of fcc2 phase.

Fig. 2 shows the microstructures of the medium entropy alloy after heat treatment. Fig. 2a and 2b present a typical dendritic morphology. Combined with XRD pattern shown in Fig. 1, it can be inferred that the alloy has a single-phase fcc structure. Fig. 2c shows that a small number of second-phase particles are precipitated in the $(Fe_{63.3}Mn_{14}Si_{9.1}Cr_{9.8}C_{3.8})_{96.5}Cu_3Ag_{0.5}$ alloy, and as the Cu content in the alloy increases, obvious second-phase appears in Fig. 2d and 2e, which are mainly distributed in the interdendritic regions. The increase in Cu content promotes the generation of Cu-enriched phase (fcc2 phase) in the alloy, which is mainly attributed to the difference of solute concentration at the solid-liquid interface. When the Cu content is high, the composition undercooling has a significant effect on the dendritic morphology, resulting in the precipitation of Cu-enriched phase. Combined with the surface EDS mapping of $(Fe_{63.3}Mn_{14}Si_{9.1}Cr_{9.8}C_{3.8})_{94.5}Cu_5Ag_{0.5}$ alloy shown in Fig. 3, it can be observed that Cu and Ag elements are significantly enriched and phase-separated, and mainly distributed in the interdendritic regions. The matrix elements Fe, Mn, Si, and Cr of the fcc1 phase are evenly distributed in the dendritic region without obvious segregation. Due to the large positive mixing enthalpy among Cu, Ag, and other main alloying elements and different atomic radii of each element, lattice distortion

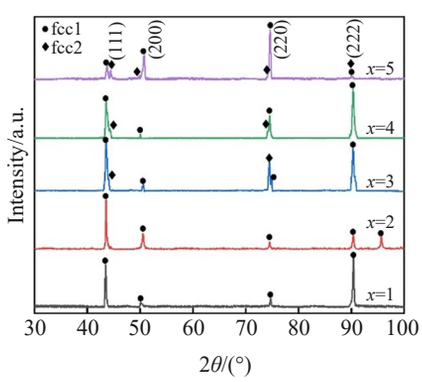

Fig.1 XRD patterns of medium entropy alloy $(Fe_{63.3}Mn_{14}Si_{9.1}Cr_{9.8}C_{3.8})_{99.5-x}Cu_xAg_{0.5}$ after heat treatment

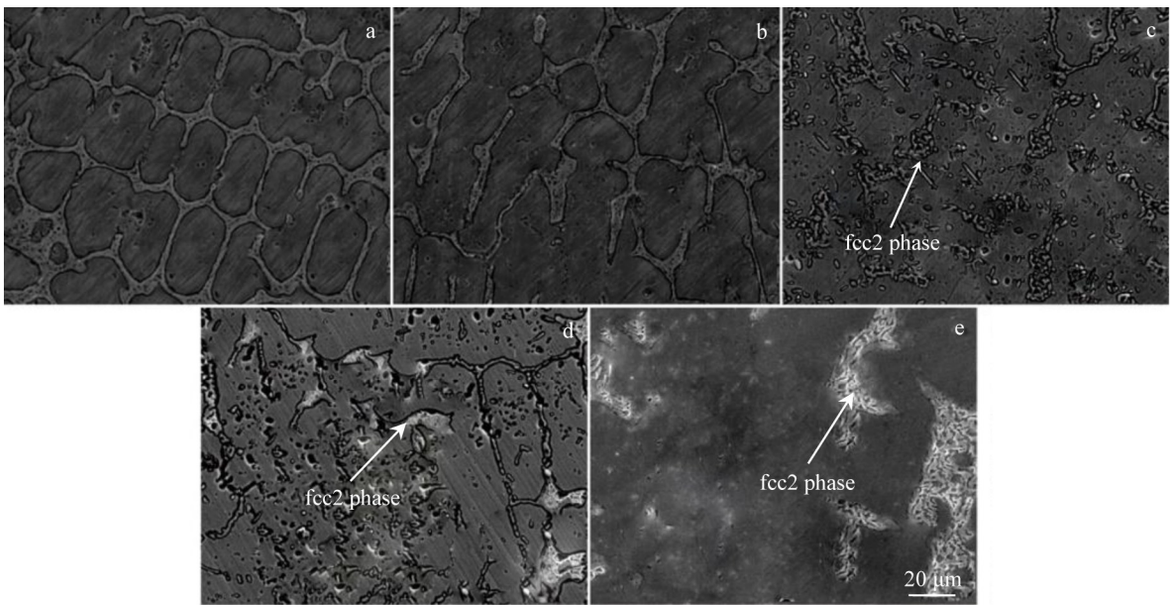

Fig.2 SEM images of medium entropy alloy $(Fe_{63.3}Mn_{14}Si_{9.1}Cr_{9.8}C_{3.8})_{99.5-x}Cu_xAg_{0.5}$ samples after heat treatment: (a) x=1, (b) x=2, (c) x=3, (d) x=4, and (e) x=5

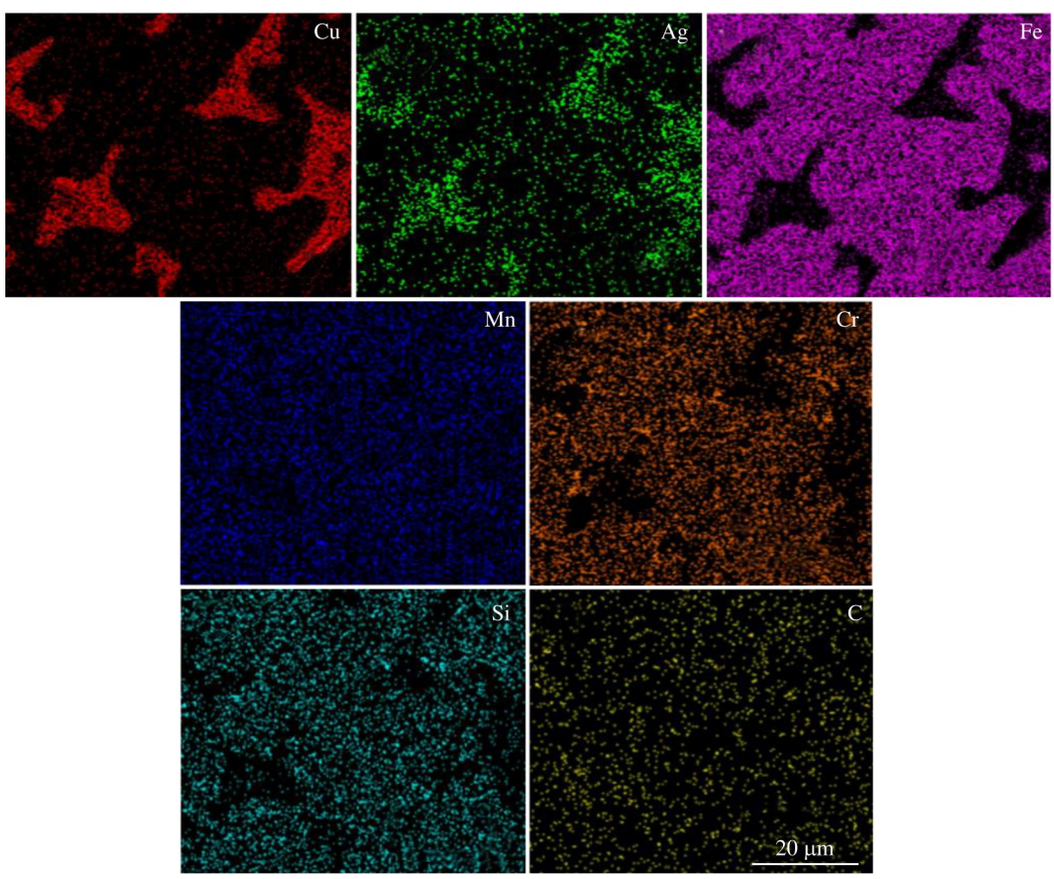

Fig.3 EDS element mappings of medium entropy alloy $(Fe_{63.3}Mn_{14}Si_{9.1}Cr_{9.8}C_{3.8})_{94.5}Cu_5Ag_{0.5}$

occurs, and the Cu and Ag elements are expelled to the interdendritic areas before solidification, resulting in the formation of Cu- and Ag-enriched fcc2 phase between the dendrites, which leads to phase separation. With the increase in Cu content in the alloy, the segregation of the Cu-enriched phase becomes more pronounced, and the Cu content is higher in the grain boundaries. Since different elements in the alloy have different atomic radii and melting points, these

differences also result in segregation during the solidification process.

2.2 Corrosion resistance of medium entropy alloy

2.2.1 Electrochemical corrosion behavior

Fig. 4 shows the potentiodynamic polarization curves of AISI304, Fe-based medium entropy alloy $Fe_{63.3}Mn_{14}Si_{9.1}Cr_{9.8}C_{3.8}$, and the alloy $(Fe_{63.3}Mn_{14}Si_{9.1}Cr_{9.8}C_{3.8})_{99.5-x}Cu_xAg_{0.5}$ in 3.5wt% NaCl solution. The corrosion potential (E_{corr}) and corrosion current density (I_{corr}) of different Cu-containing medium entropy alloys are different. After adding a certain amount of Cu and Ag elements to the matrix alloy $Fe_{63.3}Mn_{14}Si_{9.1}Cr_{9.8}C_{3.8}$, except for the alloy with x=5, the corrosion potential of alloys with x=1, x=2, x=3, and x=4 increases, while the corrosion current density decreases. Overall, the Fe-based medium entropy alloys have more positive corrosion potentials, smaller current density, and larger polarization resistance (R) compared with those of AISI304, indicating that the corrosion resistance of the alloys is better than that of AISI304 in 3.5wt% NaCl solution.

According to Table 1, when the Cu content is 1at% and 3at%, the corrosion potential and corrosion current density of the alloy are relatively close. When the Cu content is 2at%, the alloy has the highest corrosion potential of −0.297 V and the lowest corrosion current density of 1.022×10^{-7} A·cm^{-2}. However, when the Cu content increases to 5at% , the corrosion potential of the alloy decreases to −0.497 V, and the corrosion current density increases to 1.005×10^{-6} A·cm^{-2}. This indicates that adding an appropriate amount of Cu can enhance the overall corrosion resistance of the alloy, while excessive Cu content will decrease the corrosion resistance of the alloy and even have adverse effects on the corrosion resistance of the matrix alloy.

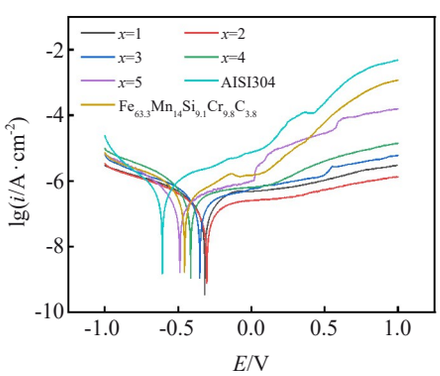

Fig. 4 Potentiodynamic polarization curves of AISI304, $Fe_{63.3}Mn_{14}Si_{9.1}Cr_{9.8}C_{3.8}$ alloy and medium entropy alloy $(Fe_{63.3}Mn_{14}Si_{9.1}Cr_{9.8}C_{3.8})_{99.5-x}Cu_xAg_{0.5}$ in 3.5wt% NaCl solution

Table 1 Parameters of potentiodynamic polarization curves of AISI304 and medium entropy alloys in 3.5wt% NaCl solution

Alloy	E_{corr}/V	I_{corr}/A·cm^{-2}	R/Ω·cm^2
AISI304	–0.558	2.622×10^{-6}	1.6096×10^{5}
x=0	–0.456	2.781×10^{-6}	3.7007×10^{5}
x=1	–0.318	3.339×10^{-7}	1.9694×10^{6}
x=2	–0.297	1.022×10^{-7}	3.8555×10^{6}
x=3	–0.344	3.989×10^{-7}	1.3789×10^{6}
x=4	–0.426	7.264×10^{-7}	1.0609×10^{6}
x=5	–0.497	1.005×10^{-6}	2.3893×10^{5}

This work aims to further investigate the corrosion behavior of alloys by conducting electrochemical impedance spectroscopy tests. Fig. 5 shows the Nyquist plot of the alloy in 3.5wt% NaCl solution. The curves exhibit typical single capacitive arc characteristics, indicating that only the electrode potential affects the alloy during the corrosion process. With an increase in Cu content, the radius of the capacitive arc initially increases and then decreases. When the Cu content is 2at% , the corresponding capacitive arc radius is the largest, indicating higher corrosion resistance and lower corrosion rate, thus demonstrating the best corrosion resistance of the alloy. However, when the Cu content reaches 5at% , the corresponding capacitive arc radius is smaller than that of the base alloy $Fe_{63.3}Mn_{14}Si_{9.1}Cr_{9.8}C_{3.8}$. Fig. 6a and 6b show the impedance-frequency and phase angle-frequency relationships of the alloy in 3.5wt% NaCl solution, respectively. It can be observed that with an increase in Cu content, the impedance modulus of the alloy initially increases and then decreases, while the phase angle initially increases and then decreases. This analysis indicates that excessive Cu addition leads to a decrease in the corrosion resistance of the alloy, thus confirming the results of the polarization curve test.

2.2.2 Corrosion morphology

Fig. 7 shows the surface morphology of the alloy $(Fe_{63.3}Mn_{14}Si_{9.1}Cr_{9.8}C_{3.8})_{99.5-x}Cu_xAg_{0.5}$ after corrosion in 3.5wt% NaCl solution. Fig. 7a and 7c show a small number of shallow corrosion pits on the surface of the alloy. Fig. 7b shows that the surface of the x=2 alloy has almost no corrosion pits. With a further increase in Cu content, the alloy shown in Fig. 7d

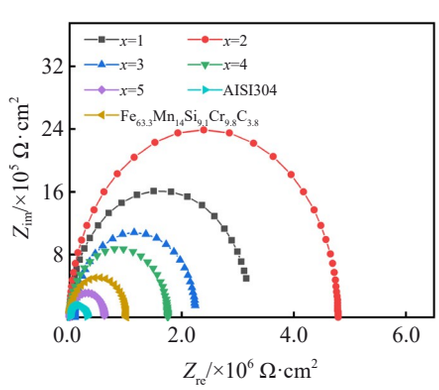

Fig. 5 Nyquist diagram of medium entropy alloy $(Fe_{63.3}Mn_{14}Si_{9.1}Cr_{9.8}C_{3.8})_{99.5-x}Cu_xAg_{0.5}$ in 3.5wt% NaCl solution

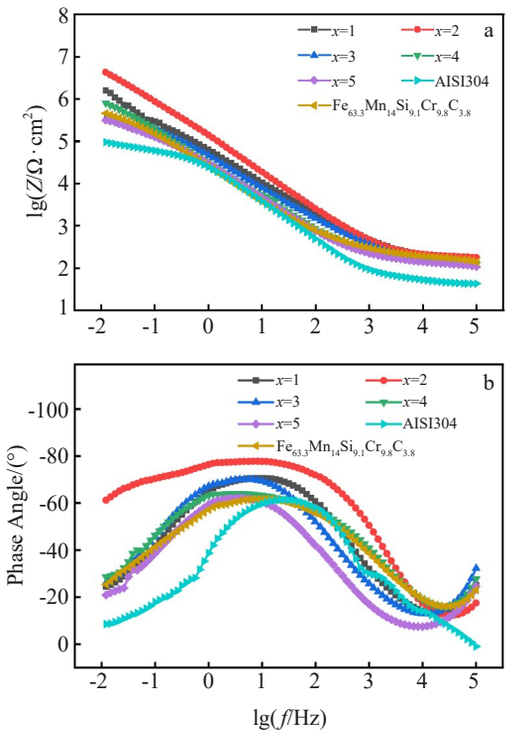

Fig. 6 Bode diagrams of AISI304, $Fe_{63.3}Mn_{14}Si_{9.1}Cr_{9.8}C_{3.8}$ alloy and medium entropy alloy $(Fe_{63.3}Mn_{14}Si_{9.1}Cr_{9.8}C_{3.8})_{99.5-x}Cu_xAg_{0.5}$ in 3.5wt% NaCl solution: (a) impedance modulus and (b) phase angle

exhibits some corroded pits. The alloy with x=5 shown in Fig. 7e has larger and deeper corrosion pits, indicating the most significant effect of the corrosive solution on the alloy. Combining the electrochemical curve and SEM results, it can be concluded that the x=5 alloy exhibits the best corrosion resistance in 3.5wt% NaCl solution.

Fig. 8 shows XPS full spectrum and fine spectra of each element (electrolyte: 3.5wt% NaCl solution) after the electrochemical corrosion of the $(Fe_{63.3}Mn_{14}Si_{9.1}Cr_{9.8}C_{3.8})_{97.5}Cu_2Ag_{0.5}$ alloy. The Na, O, and Cl elements mainly originate from the secondary introduction of the corrosion medium during the corrosion process, while the remaining elements are the components of the alloy matrix, as shown in Fig. 8a. Fig. 8b shows the Fe $2p_{3/2}$ spectra, which reveals different forms of Fe in the alloy, indicating the gradual transformation of element Fe into Fe oxides during the corrosion process[11]. Fig. 8c shows the Mn $2p_{3/2}$ spectra, of which the peak intensity corresponding to Mn_3O_4 is the highest, indicating that a large amount of Mn exists in the form of Mn_3O_4 during the corrosion process. Fig. 8d shows the Si 2p spectra, indicating that Si mainly exists in the form of oxides, as SiO has a higher binding energy. Fig. 8e shows the Cr $2p_{3/2}$ spectra, of which the highest peak is corresponding to Cr_2O_3, indicating that Cr mainly exists in the form of its oxide product Cr_2O_3 in the alloy system. Cr_2O_3 is dense and can effectively slow down the diffusion of internal ions in the passive film formed on the alloy, thereby enhancing the corrosion resistance of the alloy. Fig. 8f shows the Cu 2p spectra, which indicates that Cu mainly exists in the form of Cu_2O, as it interacts with a large amount of Cl^- in the corrosive solution and O_2 in the surrounding environment. However, as the corrosion progresses, a certain number of Cu chlorides are formed, which can destroy part of the passive film in the alloy. Combining the results of the electrochemical polarization curve and impedance tests, it can be concluded that the higher the Cu content in the alloy composition, the more the Cu chloride generated, making the alloy more susceptible to the influence of Cl^- in the corrosive solution, and resulting in a decrease in the corrosion resistance of the alloy. Fig. 8g shows the Ag $3d_{3/2}$

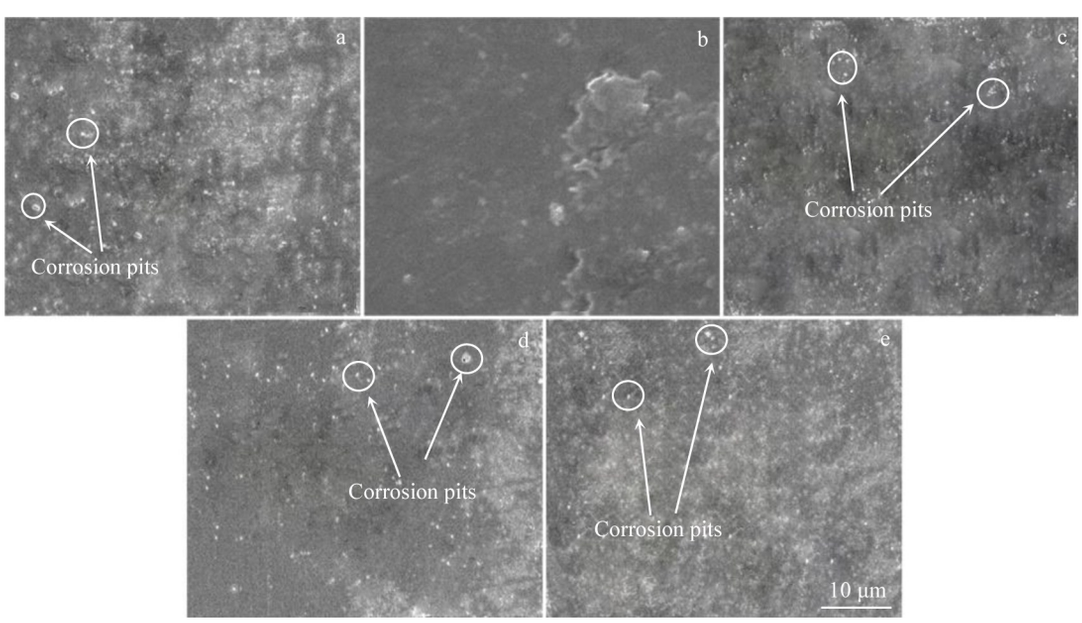

Fig.7 Corrosion morphologies of medium entropy alloy $(Fe_{63.3}Mn_{14}Si_{9.1}Cr_{9.8}C_{3.8})_{99.5-x}Cu_xAg_{0.5}$ after electrochemical corrosion in 3.5wt% NaCl solution: (a) x=1, (b) x=2, (c) x=3, (d) x=4, and (e) x=5

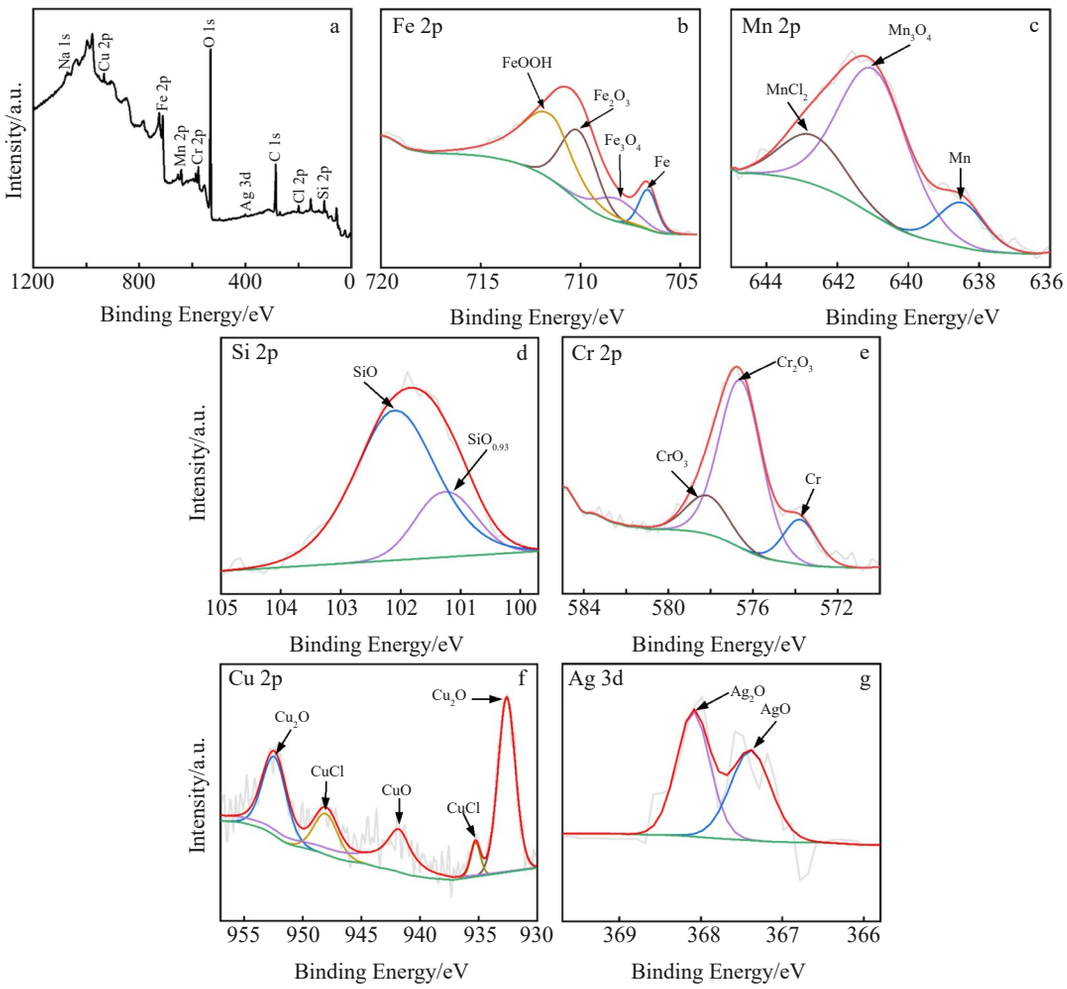

Fig.8 XPS full spectrum (a) and fine spectra (b–g) of medium entropy alloy $(Fe_{63.3}Mn_{14}Si_{9.1}Cr_{9.8}C_{3.8})_{97.5}Cu_2Ag_{0.5}$ after electrochemical corrosion

spectra, indicating that after corrosion, Ag mainly exists as stable Ag^+ and Ag^{2+} oxides on the surface of the alloy. According to XPS results, the cathode reaction during the corrosion process of the medium entropy alloy $(Fe_{63.3}Mn_{14}Si_{9.1}Cr_{9.8}C_{3.8})_{97}Cu_2Ag_{0.5}$ in 3.5wt% NaCl solution mainly involves the depolarization of oxygen[12].

$$O_2 + 2H_2O + 4e^- \rightarrow 4OH^- \quad (2)$$

As the main component of the alloy, Fe is dissolved as Fe^{2+} at the anode and reacts with OH^- generated at the cathode to form $Fe(OH)_2$. However, $Fe(OH)_2$ cannot exist stably on the alloy surface and it continues to react with O_2, leading to the formation of hydroxylated iron oxide (FeOOH). With the content of FeOOH increasing in the alloy, a small amount of Fe_3O_4 is formed when FeOOH receives electrons. The generated Fe_3O_4 is insoluble in water, resulting in a denser passive film on the surface of the substrate, effectively preventing further corrosion by Cl^- on the alloy surface[13]. The main reactions are as follows[14–15]:

$$Fe \rightarrow Fe^{2+} + 2e^- \quad (3)$$

$$Fe^{2+} + 2OH^- \rightarrow Fe(OH)_2 \quad (4)$$

$$Fe(OH)_2 + O_2 \rightarrow 2FeOOH \quad (5)$$

$$3FeOOH + e^- \rightarrow Fe_3O_4 + H_2O + OH^- \quad (6)$$

Due to the presence of Cr in the alloy, Cr can act as a cathodic activator during the corrosion process, promoting the passivation effect of the anode. At the same time, it transforms the corrosion products from crystalline to amorphous product. The amorphous component is mainly composed of Cr_2O_3, which has a compact structure and effectively reduces the diffusion channels of the alloy in the corrosive solution[16].

$$2Cr + 3H_2O \rightarrow Cr_2O_3 + 6H^+ + 6e^- \quad (7)$$

The Si element in the alloy also promotes the accumulation of Cr in the passive film. Si and Cr continuously consume oxygen in the passive layer, effectively preventing the oxidation of other elements. A small amount of Cu is added to the alloy, and during the electrochemical corrosion process, Cu combines with Cl^- in the corrosive solution to form CuCl. Since the 3.5wt% NaCl solution is a neutral chloride solution, CuCl is not easy to dissolve in the solution. It further reacts with Cl^- and H_2O, and forms a passive film of Cu_2O on the alloy surface. The main reactions are as follows[16–18]:

$$Cu + Cl^- \rightarrow CuCl + e^- \quad (8)$$

$$CuCl + Cl^- \rightarrow CuCl_2^- \quad (9)$$

$$2CuCl_2^- + H_2O \rightarrow Cu_2O + 2H^+ + 4Cl^- \quad (10)$$

During the corrosion process, Ag mainly forms Ag_2O, which stably exists on the alloy surface, thereby enhancing the corrosion resistance of the alloy. The inherent composition elements in the alloy, such as Ag, Cu, Cr, and Fe, can passivate the anode, increase the potential of the substrate, and slow down the dissolution rate of the alloy, effectively ensuring good corrosion resistance of the material in 3.5wt% NaCl solution.

2.3 Antibacterial performance of medium entropy alloy

In order to further investigate the biocorrosion resistance behavior of the alloy $(Fe_{63.3}Mn_{14}Si_{9.1}Cr_{9.8}C_{3.8})_{99.5-x}Cu_xAg_{0.5}$, it was immersed in E.coli suspension at 37 °C for 72, 120, 360, and 720 h. The biocorrosion environment was simulated, and the biocorrosion resistance of the alloy was studied by corrosion mass gain experiment. Fig. 9 shows the corrosion rate of the alloy immersed in E. coli suspension for different durations. It can be seen that the corrosion rate of the alloy increases first and then decreases. After soaking for 120 h, the corrosion rate of the alloy ($(Fe_{63.3}Mn_{14}Si_{9.1}Cr_{9.8}C_{3.8})_{99.5-x}Cu_xAg_{0.5}$ reaches the maximum, which is 4.629, 2.315, 6.944, 11.574, and 15.833 μg/(cm^2·h) for x=1, x=2, x=3, x=4, and x=5 alloys, respectively. The corrosion rate of the x=5 alloy is the largest. With prolonging the immersion time, the corrosion rate of x=4 and x=5 alloys decreases continuously, and the corrosion rate of the x=1, x=2, x=3 alloys increases first and then decreases. The immersion results show that the corrosion of the alloy in the corrosion solution is greatly different in the early stage. With the increase in immersion time, the corrosion rate of the alloy becomes slower and tends to be stable in the corrosion solution. Among the alloys, the alloy with x=2 is less affected by the corrosive liquid and has excellent biological corrosion resistance. When the Cu content is low, Cu ions interact with the surrounding O_2 to form a passive film predominantly composed of Cu_2O. As a result, the biocorrosion resistance of the alloys with x=1 and x=2 gradually increases, reaching the optimal value at x=2. However, there is also a certain amount of Cl^- in the suspension of E. coli. With the increase in Cu content, the interaction between Cu ions and the Cl^- in the corrosive solution leads to the formation of copper chloride, which promotes the degradation of the passivation film in the alloy, consequently reducing the corrosion resistance of the alloy. Therefore, the bio corrosion resistance of the alloy shows a trend of increasing first and then decreasing. This result also corresponds to the corrosion resistance of the alloy in 3.5wt% NaCl solution.

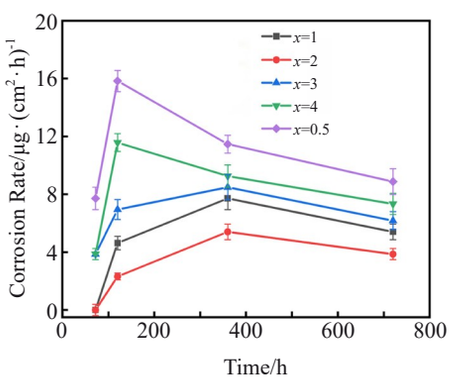

Fig.9 Corrosion rate curve of medium entropy alloy $(Fe_{63.3}Mn_{14}Si_{9.1}Cr_{9.8}C_{3.8})_{99.5-x}Cu_xAg_{0.5}$ in E.coli bacterial suspension

To investigate the antibacterial performance of the medium entropy alloy, the heat-treated alloy $(Fe_{63.3}Mn_{14}Si_{9.1}Cr_{9.8}C_{3.8})_{99.5-x}Cu_xAg_{0.5}$ was co-cultured with E. coli bacterial suspension for 12 h, and the bacteria were diluted and then placed on agar plates for cultivation. Fig. 10 shows the antibacterial test results of the alloy after co-cultivation with E. coli for 12 h. It can be seen from Fig.10b–10f that there are almost no bacterial colonies in the culture dish of the medium entropy alloy after co-cultivation for 12 h, while a large number of colonies still exist in the culture dish of the control group AISI304 (Fig.10a). After 12 h of co-cultivation, the medium entropy alloy exhibits good antibacterial

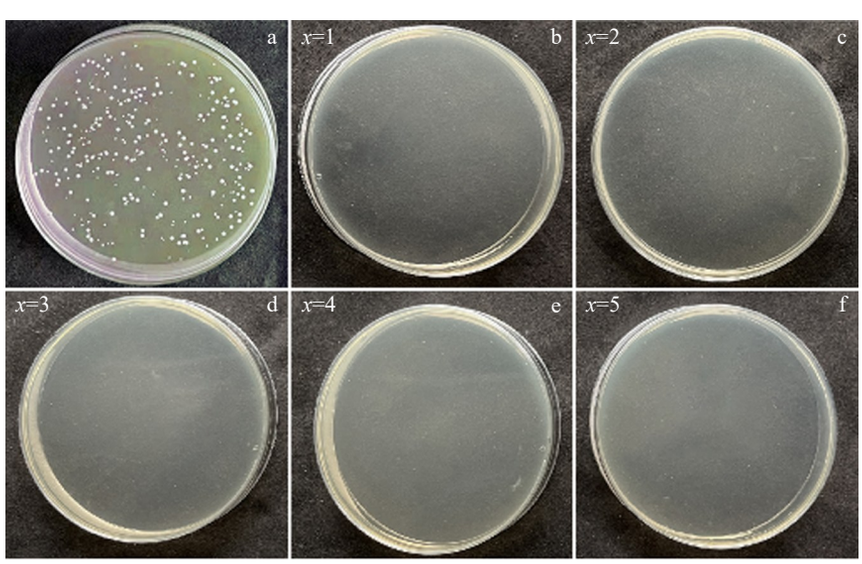

Fig.10 Plate colony culture diagrams of AISI304 (a) and medium entropy alloys (b–f) in E.coli bacterial suspension for 12 h

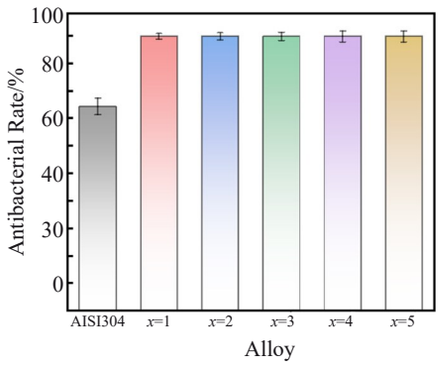

Fig. 11 Antibacterial rate of AISI304 and medium entropy alloys after interaction with E.coli bacterial suspension for 12 h

performance, effectively inhibiting the formation of bacterial colonies. Fig.11 shows the antibacterial rate of the alloy. After 12 h of cultivation, the antibacterial rate of the control sample AISI304 is 74.20%, while the antibacterial rates are 99.90%, 99.92%, 99.92%, 99.93%, and 99.94% for x=1, x=2, x=3, x=4, and x=5 alloys, respectively, indicating excellent antibacterial performance. After 12 h of cultivation, the antibacterial rate of the medium entropy alloy is significantly improved, and x=5 alloy exhibits the strongest antibacterial ability. This is mainly because with the increase in Cu content, the quantity of Cu-enriched phase in the alloy gradually increases and the size becomes smaller. This smaller-sized antibacterial phase is dispersed throughout the matrix, which is more conducive to the enhancement of the antibacterial performance of the alloy, thereby increasing the antibacterial rate of the alloy.

3 Conclusions

1) The microstructure of the alloy $(Fe_{63.3}Mn_{14}Si_{9.1}Cr_{9.8}C_{3.8})_{99.5-x}Cu_xAg_{0.5}$ shows that with the increase in Cu content, Cu element is significantly enriched and mainly distributed in the interdendritic region, resulting in the formation of Cu- and Ag-enriched fcc2 phases in the interdendritic region, leading to phase separation.

2) The corrosion resistance of the alloy $(Fe_{63.3}Mn_{14}Si_{9.1}Cr_{9.8}C_{3.8})_{99.5-x}Cu_xAg_{0.5}$ is superior to that of AISI304. With the increase in Cu content, the corrosion potential of the alloy first increases and then decreases, the corrosion current density first decreases and then increases, and the impedance arc radius first increases and then decreases, indicating that the corrosion resistance of the alloy first improves and then decreases. Among them, the x=5 alloy exhibits the best corrosion resistance. The addition of an appropriate amount of Cu can enhance the overall corrosion resistance of the alloy, while excessive amount of Cu element will decrease the corrosion resistance of the alloy.

3) The corrosion rate of the alloy $(Fe_{63.3}Mn_{14}Si_{9.1}Cr_{9.8}C_{3.8})_{99.5-x}Cu_xAg_{0.5}$ in E. coli suspension shows a trend of increasing first and then decreasing. The alloy with x=2 is less affected by the corrosive solution and has excellent resistance to biocorrosion. The x=5 alloy has the poorest resistance to biocorrosion but the best antibacterial performance, with an antibacterial rate up to 99.94%.

References

1 Shu Xiaoyong, Qiu Panpan, Hu Linli *et al. Rare Metal Materials and Engineering*[J], 2023, 52(2): 551 (in Chinese)

2 Yan Fei, Du Xinghao, Jin Chengyan *et al*. *Rare Metal Materials and Engineering*[J], 2023, 52(1): 179 (in Chinese)

3 Zhao Yanchun, Zhang Minya, Zhang Linhao *et al. Rare Metal Materials and Engineering*[J], 2022, 51(11): 4146 (in Chinese)

4 Ren B, Liu Z X, Li D M *et al. Materials and Corrosion*[J], 2012, 63(9): 828

5 Mei Jinna, Xue Fei, Wu Tiandong *et al*. *Rare Metal Materials and Engineering*[J], 2022, 51(2): 429

6 Muangtong P, Rodchanarowan A, Chaysuwan D *et al. Corrosion Science*[J], 2020, 172: 108740

7 Hsu Y J, Chiang W C, Wu J K. *Materials Chemistry & Physics*[J], 2005, 92(1): 112

8 Kato M, Nishimoto M, Muto I *et al. Corrosion Science*[J], 2023, 213: 110982

9 Luo Xinrui, Zheng Dandan, Wang Hui *et al*. *Rare Metal Materials and Engineering*[J], 2022, 51(12): 4542 (in Chinese)

10 Feng R, Liaw P K, Gao M C *et al. Computational Materials*[J], 2017, 3(1): 50

11 Ai Z Y, Jiang J Y, Sun W *et al*. *Journal of Southeast University*[J], 2016, 46(1): 152

12 Ma T, Li H R, Gao J X *et al. Journal of Materials Research*[J], 2019, 33(3): 225

13 Chen H L, Chen S H, Wei Y. *Materials Protection*[J], 2007, 344(9): 20

14 Zhang Hao, Du Nan, Zhou Wenjie *et al. Chinese Journal of Corrosion and Protection*[J], 2020, 40(6): 517 (in Chinese)

15 Hu Jiafu, Xie Chunxiao, Tao Pingjun. *Material Bulletin*[J], 2022(S1): 1 (in Chinese)

16 Zeng Delu. *Study on Corrosion Resistance of Aluminum Brass with Trace Cr and Co Addition*[D]. Hunan: South Central University, 2014: 22 (in Chinese)

17 Cao Z Q, Yin X T, Jia Z Q *et al. Transactions of Nonferrous Metals Society of China*[J], 2019, 29(7): 1495

18 Luo W, Qian C, Wu X J *et al. Materials Science and Engineering A*[J], 2007, 452: 524

Cu含量对铁基中熵合金耐腐蚀及抗菌性能的影响

赵燕春[1,2]，宋海转[1]，马虎文[1]，胡若楠[1]，冯　力[1,2]，段望春[3]，Liaw Peter K[4]

(1. 兰州理工大学 省部共建有色金属加工与再利用国家重点实验室，甘肃 兰州 730050)

(2. 兰州理工大学 温州泵阀工程研究院，浙江 温州 325105)

(3. 兰州资源环境职业技术大学，甘肃 兰州 730123)

(4. 田纳西大学 材料系，美国 诺克斯维尔 TN 37996)

摘　要：采用水冷铜坩埚磁悬浮真空熔炼炉制备了$(Fe_{63.3}Mn_{14}Si_{9.1}Cr_{9.8}C_{3.8})_{99.5-x}Cu_xAg_{0.5}$ (x=1，2，3，4，5，at%)合金，并对合金试样进行抗菌时效处理，研究Cu含量对合金耐腐蚀性能以及抗菌性能的影响。结果表明，经过固溶时效处理后的中熵合金均为fcc结构，随着Cu含量的提高，fcc1富铁基体上逐渐析出了富Cu和富Ag的fcc2相。合金在3.5%（质量分数）NaCl溶液中的耐腐蚀性能优于AISI304。随Cu含量的增加，腐蚀电流密度先减小而后增加，容抗弧半径先增大后减小，表明合金的耐腐蚀性能先增强后减弱。合金在大肠杆菌悬浮液中的腐蚀速率呈现出先增大后减小的趋势，x=2合金的耐生物腐蚀能力最优，而抗菌性能和腐蚀性能存在倒置关系。富Cu和富Ag的fcc2相能有效提升合金的抗菌性能，x=5合金的抗菌性能最优，抗菌率达到99.94%.

关键词：中熵合金；微观组织；腐蚀性能；抗菌性能

作者简介：赵燕春，女，1984年生，博士，教授，兰州理工大学省部共建有色金属先进加工与再利用国家重点实验室，甘肃 兰州 730050，E-mail：zhaoyanchun@edu.lut.cn